Vol 16 No 11, November 2007
1009-1963/2007/16(11)/3345-07

Chinese Physics

© 2007 Chin. Phys. Soc.
and IOP Publishing Ltd

The effect of the attractive well of the potential energy surface for Ne–HCl on rotationally inelastic partial wave cross sections*

Yu Chun-Ri(余春日)[a)b)d)†], Shi Shou-Hua(史守华)[b)],
Wang Rong-Kai(汪荣凯)[c)d)], and Yang Xiang-Dong(杨向东)[d)‡]

[a)] *School of Physics & Electric Engineering, Anqing Teachers College, Anqing* 246011, *China*
[b)] *School of Physics and Materials Science, Anhui University, Hefei* 230039, *China*
[c)] *School of Science, Guizhou Normal University, Guiyang* 550001, *China*
[d)] *Institute of Atomic and Molecular Physics, Sichuan University, Chengdu* 610065, *China*

(Received 18 November 2006; revised manuscript received 25 June 2007)

An interaction potential of the Ne–HCl van der Waals complex is obtained by utilizing the Huxley analytic potential function to fit the accurate interaction energy data, which have been computed at the coupled cluster singles and doubles including connected triple excitations level and with the augmented correlation consistent polarized valence quintuple zeta basis set extended with a set of 3s3p2d1f1g mid-bond functions [CCSD (T) /aug-cc-pV5Z-33211]. The close coupling calculation of state-to-state partial cross sections for collision of Ne with HCl is first performed by employing the fitted interaction potential. This calculation is performed at the incident energies: 40, 60, 75 and 100 meV, separately. The effects of the long-range attractive and the short-range anisotropic interactions on the inelastic state-to-state partial cross sections are discussed in detail. Two maxima are present in the rotationally inelastic partial cross sections and they originate from different mechanisms.

Keywords: potential energy surface, inelastic partial wave cross sections, close-coupling approach, Ne–HCl complex

PACC: 3440, 3430, 3450E

1. Introduction

The inelastic vibrational–rotational energy transfer in weakly interacting molecules can provide a great deal of information for reference in the study of molecular spectrum, vibrational and rotational energy level structures of molecules, thermal scattering in mixture gases, gas phase relaxation, chemical reaction dynamics, interactions between laser and matter, intramolecular vibrational redistribution or vibrational predissociation, and cooling process in planetary space. On account of the significance of collision energy transfer in the field, the corresponding theoretical and experimental investigations have been carrying on.[1−11] There exists a vast literature dealing with the interaction and dynamics between He atoms and hydrogen halide molecules.[12−24]

In contrast, the investigation of Ne–HCl van der Waals complex is rare. Barton *et al*[25] measured the microwave and radiofrequency stark spectra of the NeDCl complex for the first time using a molecular beam electric resonance technique. The results were used by Huston and Howard[26] to obtain an intermolecular potential energy surface (PES) for the complex by least-squares fitting the molecular beam spectra. In 1988, Lovejoy and Nesbitt[27] obtained the near-infrared spectrum of jet-cooled NeHCl. Based on their results, an intermolecular potential (H6) was obtained by Hutson.[28] The first theoretical PES was evaluated by Dudley *et al*[29] from CCSD (T)/cc-pVTZ interaction energies. Recently, another theoretical PES has been evaluated for this complex by Li *et al*[30] using the CCSD (T)/aug-cc-pVTZ extended with a set of 3s3p2d midbond functions. However, the computed rovibrational spectra from the theoretical PES do not agree well with the experimental

*Project supported by the National Natural Science Foundation of China (Grant Nos 10676025 and 10574096), the Discipline Foundation of Anqing Teachers College of China (Grant No 044-k06016000007) and the Anhui Provincial Natural Science Foundation of China (Grant No 20050610010).

†E-mail: cryu2@126.com, cryu@aqtc.edu.cn
‡Corresponding author. E-mail: xdyang@scu.edu.cn

data. In order to improve these results, Fajın and coworkers[31] calculated the PES obtained at the coupled cluster singles and doubles (including connected triple) excitation levels, with the augmented correlation consistent polarized valence quintuple zeta basis set extended with a set of 3s3p2d1f1g midbond functions for the rigid Ne–HCl system. The PES of Ne–HCl is characterized by two linear minima, which are located in the linear Ne–HCl ($\theta = 0°$) and Ne–ClH ($\theta = 180°$) geometry in Jacobian coordinates, respectively. From the PES they also evaluated the rovibrational spectra for different isotopic species. These computed results agree qualitatively well with the experimental data available.

To the best of our knowledge, there is neither the experimental study nor the quantum dynamical study on the collision of Ne–HCl reported in literature. In this paper, we report the results of the quantum dynamical investigation on the basis of Fajın's PES for this system. In the following section we briefly review the accurate quantum close-coupling approach used in our calculation, and then the rotationally inelastic partial wave scattering cross sections based on the PES mentioned above and a discussion are presented in detail in Section 3. Conclusions will be presented in Section 4. We believe that the present results are beneficial for further experimental and theoretical studies on the Ne–HCl complex.

2. The quantum close-coupling approach

According to the close-coupling approach,[32] the differential cross section for the collision process between an atom (A) and a diatomic molecule (BC): A+BC (ν_α, j_α) → A+BC (ν_β, j_β) is given by

$$\frac{\mathrm{d}\sigma_{\nu_\alpha j_\alpha \to \nu_\beta j_\beta}}{\mathrm{d}\Omega} = \frac{1}{(2j_\alpha + 1)} \frac{k_\beta}{k_\alpha} \sum_{M_\alpha M_\beta} \left| f_{\nu_\beta j_\beta M_\beta, \nu_\alpha j_\alpha M_\alpha}(\theta, \phi) \right|^2, \tag{1}$$

where ν is the molecular vibrational quantum number, j is the rotational quantum number, M is the quantum number of projection of rotational quantum number onto a space-fixed axis, and k represents the wave vector.

The scattering amplitude from the initial state ($\nu_\alpha j_\alpha M_\alpha$) to the final state ($\nu_\beta j_\beta M_\beta$) is

$$f_{\upsilon_\beta j_\beta M_\beta, \upsilon_\alpha j_\alpha M_\alpha}(\theta, \phi) = \left(\frac{4\pi}{k_\alpha k_\beta} \right)^{\frac{1}{2}} \times \sum_{l_\beta} [2l_\beta + 1]^{1/2} A_{l_\beta}(\upsilon_\alpha j_\alpha M_\alpha \to \upsilon_\beta j_\beta M_\beta) Y_{l_\beta M_\alpha \to M_\beta}(\theta, \phi) \tag{2}$$

with

$$A_{l_\beta}(\upsilon_\alpha j_\alpha M_\alpha \to \upsilon_\beta j_\beta M_\beta) = \sum_J \langle l_\beta M_\alpha - M_\beta j_\beta M_\beta \, | J M_\alpha \rangle \, T^J_{\upsilon_\alpha j_\alpha l_\alpha, \upsilon_\beta j_\beta M_\beta}, \tag{3}$$

where l is the quantum number of orbital angular momentum, J denotes the quantum number of total angular momentum, $Y_{l_\beta M_\alpha \to M_\beta}(\theta, \phi)$ is the spherical harmonics and $T^J_{\upsilon_\alpha j_\alpha l_\alpha, \upsilon_\beta j_\beta M_\beta}$ is the transition matrix element.

The total partial cross section (PCS) for the collision process: A+BC (ν_α, j_α) → A+BC (ν_β, j_β) is given by

$$\sigma^J_{\nu_\alpha j_\alpha \to \nu_\beta j_\beta} = \frac{1}{2j_\alpha + 1} \frac{4\pi}{K^2_\alpha} \sum_{l_\beta M_\alpha} (2l_\beta + 1) \times \left| T^J_{\upsilon_\alpha j_\alpha l_\alpha, \upsilon_\beta j_\beta M_\beta} \right|^2. \tag{4}$$

3. Results and discussion

3.1. Potential energy surface for Ne–HCl system

Ab initio calculation of the interaction energy between Ne and HCl has been performed by Fajın and co-workers.[31] A set of 113 intermolecular geometries on the PES were fitted into an analytic expression, from which the detail of the PES can be analysed. The behaviour of the potential surface as a function of the Ne–HCl separation for several relative orientations is shown in Fig.1. The corresponding potential param-

eters are shown in Table 1. Here, θ is the selected orientation angle, $R_{\rm m}$ denotes the corresponding position of the well, R_0 denotes the positions where the interaction potential is zero.

Table 1. The potential parameters for Ne–HCl complex at selected directions.

$\theta/(^\circ)$	0	20	40	60	80	90	100	100.18	120	140	160	180
$V_{\rm m}$/meV	−8.289	−7.990	−7.293	−6.194	−5.421	−5.272	−5.217	−5.216	−5.326	−5.943	−7.215	−8.072
$R_{\rm m}$/nm	0.3833	0.3777	0.3664	0.3643	0.3697	0.3711	0.3712	0.3712	0.3680	0.3590	0.3463	0.3398
R_0/nm	0.3465	0.3404	0.3280	0.3245	0.3294	0.3310	0.3313	0.3313	0.3286	0.3205	0.3090	0.3032

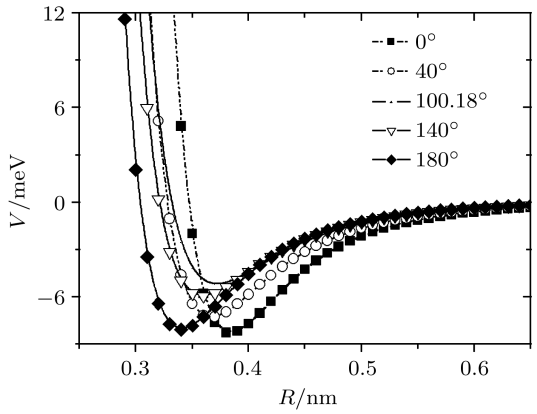


Fig.1. Section of the Ne–HCl potential energy surface associated with different Jacobian angles.

We can see that the absolute minimum on the PES has an energy of –8.289 meV and it is located at $\theta = 0^\circ$ (corresponding to the Ne–H–Cl linear configuration) with the Ne atom at a distance of 0.3833 nm with respect to the HCl centre of mass. The surface has a second minimum at $\theta = 180^\circ$ (corresponding to the Ne–Cl–H linear configuration), with the Ne atom at a distance of 0.3398 nm with respect to the HCl centre of mass and an energy of −8.072 meV. The saddle point is located at $R = 0.3712$ nm and $\theta = 100.18^\circ$ with an energy of −5.216 meV. The Ne–H–Cl and Ne–Cl–H linear geometry structures have interaction energies very close to each other. This is understandable because the electron density of the HCl monomer is substantially smaller in this direction than perpendicular to the internuclear axis, so that the intermolecular repulsion at a given distance is weaker for the linear Ne–Cl–H geometry than for a T-shaped configuration. This demonstrates that the interaction potential is weakly angular anisotropic. We can see from Fig.1 that the attractive wells are pronounced at each angle compared with that of the He–HCl system.[17]

In order to investigate quantum dynamics of Ne–HCl conveniently, we expand its interaction potential in Legendre polynomials as

$$V(R,r,\theta) = \sum_{\lambda} V_\lambda(R,r) P_\lambda(\cos\theta),$$
$$\lambda = 0,\ 1,\ 2, \cdots, \tag{5}$$

where R, r and θ are the conventional Jacobian coordinates of the Ne position vector $\boldsymbol{R}$ with the origin at the HCl centre of mass, R represents the length of vector $\boldsymbol{R}$, and θ the angle this vector makes with the HCl molecule, taking as $\theta = 0^\circ$ the linear Ne–HCl configuration, r is the bond length of HCl (fixed at its equilibrium value of 0.12838 nm). The radial coefficients $V_\lambda(R)$ of the Ne–HCl potential energy surface can be expressed employing the Huxley analytic function[33]

$$\begin{aligned} V_\lambda(R) \ = \ & A\left(1 + \sum_{n=1}^{3} a_n R^n\right)\exp(-a_4 R) \\ & - \tanh(R - R_{\rm m}/2)\left(C_6 R^{-6} + C_8 R^{-8}\right. \\ & \left. + C_{10} R^{-10}\right), \end{aligned} \tag{6}$$

where $\tanh x = \left(\dfrac{e^x - e^{-x}}{e^x + e^{-x}}\right)$, $R_{\rm m}$ is the position of the potential well, A, a_1, a_2, a_3, a_4, C_6, C_8 and C_{10} are the adjustable parameters, which are shown in Table 2. Here, ε denotes the depth of the potential well, its value was obtained using Eq.(6).

Table 2. The fitted potential parameters for Ne–HCl complex.

coefficient	ε /meV	$R_{\rm m}$ /nm	A /meV	a_1 /10^8 nm^{-1}	a_2 /10^9 nm^{-2}	a_3 /10^9 nm^{-3}	a_4 /10 nm^{-1}	C_6 /10^{-6} eV·nm^6	C_8 / 10^{-6} eV·nm^8	C_{10} / 10^{-8} eV·nm^{10}
V_0	−5.929	0.3675	0.2643	−0.2451	−0.6517	13.7997	4.6568	13.2156	2.2706	0.3895
V_1	−1.014	0.3884	3.8981	2.4560	−2.3500	6.4435	5.2509	−1.4035	2.0622	−14.4388
V_2	−1.443	0.3615	1.2816	1.2440	−1.8650	9.8413	5.2702	−3.9781	1.6371	−1.5028
V_3	−0.556	0.4045	0.8422	1.6370	−2.0000	8.4869	4.8799	−3.1128	1.5658	−2.3113
V_4	−0.329	0.4046	2.0480	2.3720	−2.2050	6.0454	5.0907	−3.9604	1.7608	−10.3764

3.2. The partial cross sections for the scattering of the Ne–HCl

Based on the above fitted potential, we have calculated the state-to-state rotational excitation partial wave cross sections from initial state $j = 0$ to final state j' for the collision of HCl with Ne at the incident energies: 40, 60, 75 and 100 meV, separately. The calculated partial wave number is 190 for each of the incident energies. We assume that the partial wave is convergent when the value of partial wave cross section reaches $10^{-4}a_0^2$, where a_0 is the Born radius.

In order to understand better the collision energy transfer process, we inspect the contribution of each inelastic partial wave to the total inelastic partial cross section (PCS). In Figs.2 and 3 we show respectively the variations of the total inelastic PCS and state-to-state excitation PCS with the increase of the quantum number J of total angular momentum at the collision energy of 100 meV. The typical character of the curves

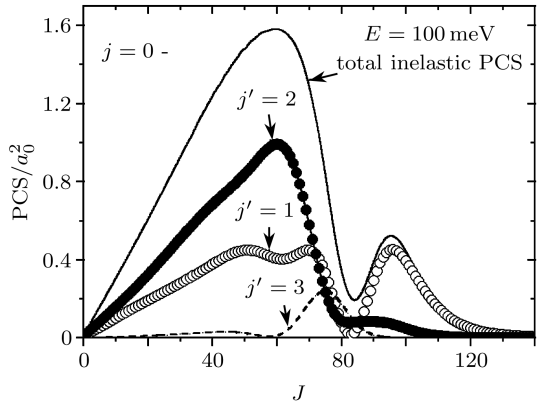


Fig.2. The total inelastic and state-to-state PCSs from the initial state $j = 0$ to final state j' as functions of total angular momentum J at the incident energy of 100 meV.

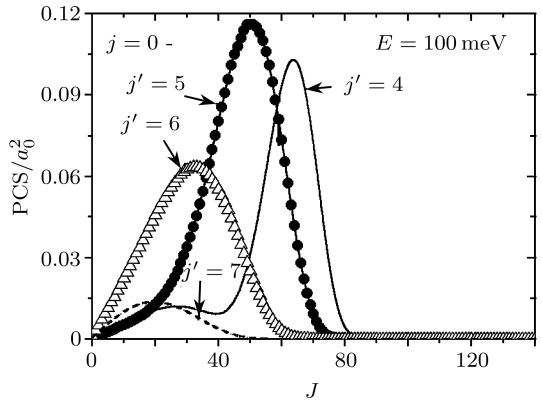


Fig.3. The state-to-state PCSs from the initial state $j = 0$ to final state j' as functions of total angular momentum J at the incident energy of 100 meV.

is that there are two peaks for the total inelastic PCS and the lower rotational transitions of $j = 0 \to j' = 1$, 2, but only one peak for the higher rotational transitions of $j = 0 \to j' = 3$, 4, 5, 6, 7. Similar character has been observed for He–HF, He–HBr and He–HCl scatterings.[13,17,22] They result from the interference of quantum mechanical waves, which are associated with the different classical trajectories that lead to the same angular momentum transfer. Since the molecule is initially in ground rotational state $j = 0$, the quantum number J of total angular momentum equals the quantum number l of orbital angular momentum of the incident channel, and these plots also represent PCSs as functions of the quantum number l of initial orbital angular momentum. Classically, impact parameter can be associated with a given l using the relation[34]

$$b_l \sim \hbar l/P = \hbar l/\sqrt{2\mu E}, \tag{7}$$

where μ is the reduced mass of the Ne–HCl system, E is the total collision energy.

In terms of Eq.(7), the calculated impact parameters corresponding to the characteristic value J of the total inelastic PCS are as follows: $b_{59} = 0.237$ nm, $b_{84} = 0.337$ nm, $b_{95} = 0.381$ nm. From Table 1 we notice that b_{84} and b_{95} corresponding to the minimum and tail maximum in the total inelastic PCS are almost equal to the locations of the short-range and long-range attractive wells of the PES, respectively. And b_{59} corresponding to the main peak is less than 0.3032 nm (the corresponding characteristic value J is 76), which is the position where the interaction potential is zero at $\theta = 180°$. These mean that orbital angular momenta from 0 to 76 correspond to the scatterings in the hard repulsive wall of the potential, those from 76 to 84 correspond to the collisions in the region where both the short-range attractive and short-range repulsive parts of the potential contribute to the PCSs, For $l > 84$, the scattering is determined by the long-range attractive part of the potential.

Based on the above argument, we suggest a reasonable interpretation for the behaviour of the collision dynamics shown in Figs.2 and 3 as follows. First of all, the total inelastic PCS comes mainly from the transitions of $j = 0 \to j' = 1$, 2, and the contribution of the former to the tail maximum at high J is predominant over that of the latter; yet the contribution of the latter to the main peak is predominant over that of the former. It is understandable that the PCS coming from the transition of $j = 0 \to j' = 1$ is de-

termined by the long-range attractive and anisotropic short-range parts of the PES. However, for the transition of $j = 0 \to j' = 2$, the contribution of the long-range attractive part of the PES to the PCS is extremely small. The PCSs coming from the transitions of $j = 0 \to j' \geq 3$ are determined almost by the anisotropic short-range part of the PES. Secondly, the main peaks of the state–to-state excitation PCS lie between $J = 0$ and $J = 76$, and the contribution of the transition of $j = 0 \to j' = 2$ to the main peak of the total inelastic PCS is the largest among all the state-to-state excitation transitions, which correspond to the hard repulsive part of the potential. This demonstrates that $J = 0$ through 76 is very efficient in exciting HCl molecule from $j = 0$ to $j' = 2$. As for the J from 76 to 84, the short-range attractive well on the Cl side of the potential also contributes to a considerable quantity of PCSs, except for the contributions from repulsive part. When J arrives at 84, the net contribution reaches its minimum.

Figure 4 shows the PCSs for the same rotational transitions as in Figs.2 and 3 but at the collision energy of 60 meV. It is very clear that the behaviour of

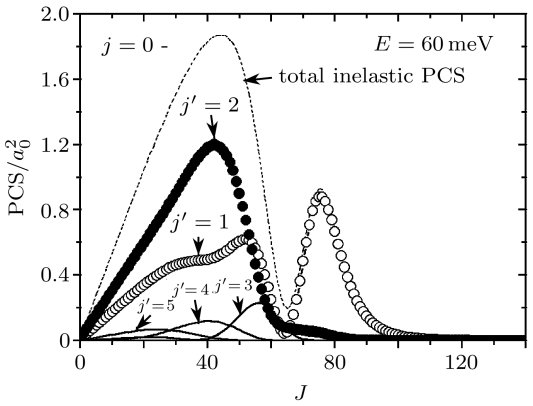


Fig.4. The total inelastic and state-to-state PCSs from the initial $j = 0$ to final state j' as functions of total angular momentum J at the incident energy of 60 meV.

the PCSs as a function of the total angular momentum number J is similar to that in the case of $E = 100$ meV, as shown in Figs.2 and 3. For example, although the positions of the two peaks and of the minimum in the inelastic transition $j = 0 \to j' = 1$ are different in the two cases, but they correspond to almost the same impact parameters, namely $b_{52} = 0.269$ nm, $b_{64} = 0.331$ nm, $b_{76} = 0.394$ nm for $E = 60$ meV; $b_{69} = 0.277$ nm, $b_{83} = 0.333$ nm, $b_{96} = 0.385$ nm for $E = 100$ meV. This means that the collision parameters sample the same portions of the PES. As the collision energy increases, the Ne atom penetrates easily into the potential, so the values of impact parameters related to the main peaks increase slightly. In addition, we see again that the long-range attractive well has a significant contribution to the tail maximum for the lower Δj inelastic transitions, whereas it does not exist for the higher inelastic transitions, as seen from Figs.2 and 3. Thus, we consider the interpretation for the collision dynamics of $E = 60$ meV in Fig.4 to be similar to that at $E = 100$ meV in Figs.2 and 3.

Figure 5 displays the variation of the total inelastic PCS for Ne–HCl collision with the increase of total angular quantum number J at different collision energies. The characteristic value J and impact parameters corresponding to the two peaks and the minimum of each inelastic PCS are shown in Table 3. From Fig.5 and Table 3, once again we can see that although the positions of the two peaks and the minimum in the inelastic PCS are different in the four cases, they correspond to almost the same impact parameters. For instance, for the minima of the inelastic PCSs, $b_{53} = 0.336$ nm for $E = 40$ meV, $b_{65} = 0.337$ nm for $E = 60$ meV, $b_{73} = 0.338$ nm for $E = 75$ meV, $b_{84} = 0.337$ nm for $E = 100$ meV. As the collision energy increases, the values of impact parameters related to the main peaks increase slightly, whereas those related to the tail maxima decrease slightly.

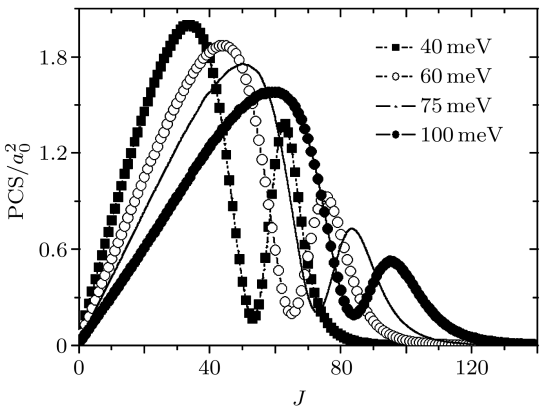


Fig.5. The total inelastic PCSs as functions of total angular momentum quantum number J at the collision energies: 40, 60, 75 and 100 meV. The HCl molecule is initially in the state of $j = 0$.

Another typical feature is that with the increase of the incident energy, the tail maximum becomes weaker and weaker as the corresponding quantum number J increases. For instance,

$E = 40$ meV, $l = 63$, $\sigma_{\text{tail}}^{\max} = 1.38a_0^2$; $E = 60$ meV, $l = 75$, $\sigma_{\text{tail}}^{\max} = 0.929a_0^2$;

$E = 75$ meV, $l = 83$, $\sigma_{\text{tail}}^{\max} = 0.731a_0^2$; $E = 100$ meV, $l = 95$, $\sigma_{\text{tail}}^{\max} = 0.525a_0^2$.

This phenomenon can be explained as follows: the lower the incident energy is, the more prominent the wave property of the scattering particle is. When the angular quantum of the incident particle is large enough, the particle cannot interact with the scattering potential field from the viewpoint of classical scattering, but the particle can still be scattered by the potential field because of quantum effect.

Table 3. The characteristic value J and impact parameters corresponding to the two peaks and the minimum of each inelastic PCS at different collision energies for Ne–HCl complex.

40 meV	main peak	minimum	tail max	60 meV	main peak	minimum	tail max
$l(J)$	34	53	63	$l(J)$	44	65	75
b_l/nm	0.216	0.336	0.400	b_l/nm	0.228	0.337	0.388
75 meV	main peak	minimum	tail max	100 meV	main peak	minimum	tail max
$l(J)$	50	73	83	$l(J)$	59	84	95
b_l/nm	0.232	0.338	0.384	b_l/nm	0.237	0.337	0.381

4. Conclusions

In this work, a new intermolecular interaction potential of the Ne–HCl van der Waals complex is obtained by utilizing the Huxley analytic function to fit an accurate *ab initio* CCSD (T)/aug-cc-pV5Z-33211 data. The close coupling calculation of state-to-state excitation PCSs for the collision of Ne with HCl is first performed by adopting the fitted interaction potential. Based on the discussion above, we can draw some conclusions as follows:

(1) Both long-range attractive and short-range anisotropic interactions are found to contribute to total inelastic excitation PCS of the low rotational states. The long-range attraction results in the tail maximum at high J. The short-range interaction results in the main peak.

(2) The long-range attractive well makes the significant contribution to the PCSs, especially the tail maximum for $j = 0 \rightarrow j' = 1$ inelastic transitions, whereas no contribution is to the $j' \geq 3$ inelastic transitions.

(3) The short-range (the repulsive and attractive) interaction makes the significant contribution to PCSs, especially the main peak for $j = 0 \rightarrow j' = 2$. As for the transition of $j' \geq 3$, the short-range interaction plays a key role in the inelastic excitation.

(4) A perfect compensation exists between the short-range anisotropic, which is predominantly repulsive, and the long-range attractive interaction, so that they cancel each other out, resulting in a deep minimum in the inelastic PCS.

(5) The variations of the rotational excitation partial wave cross sections with the partial wave number J are similar for the four incident energies considered here. Although the positions of the two peaks and the minimum are different in the four cases, they correspond to almost the same impact parameters. With the increase of the incident energy, the tail maximum becomes weaker and weaker as the corresponding quantum number J increases.

We believe that this work may provide some information for further scattering experiments and theoretical study of weakly interacting molecules.[35−37]

References

[1] Wang R K, Linghu R F and Yang X D 2007 *Acta Phys. Sin.* **56** 2067 (in Chinese)

[2] Sun J F, Zhang J C and Wang J M 2006 *Chin. Phys.* **15** 531

[3] Menapace J A and Bernstein E R 1987 *J. Phys. Chem.* **91** 2533

[4] Yang X D, Zhang J Y and Jing F J 1998 *Chin. Phys. Lett.* **15** 19

[5] Shi D H, Sun J F, Zhu Z L and Liu R F 2006 *Acta Phys. Sin.* **55** 2228 (in Chinese)

[6] Hu B T 2007 *Chin. Phys.* **16** 1285

[7] Roman V K, Nikola M, Alexei A B and Sture N 2001 *J. Chem. Phys.* **114** 1249

[8] Li Y Q, Song P, Chen Y H, Wang W L and Ma F C 2005 *Commun. Theor. Phys.* **44** 347

[9] Xu C X, Xie D Q and Zhang D H 2006 *Chin. J. Chem. Phys.* **19** 96

[10] Sun G H and Yang X D 2002 *Acta Phys. Sin.* **51** 506 (in Chinese)

[11] Zheng D S and Guo X K 2004 *Acta Phys. Sin.* **53** 3347 (in Chinese)

[12] Moszynski R, Wormer P E S, Jeziorski B and Avoird A 1994 *J. Chem. Phys.* **101** 2811

[13] Zeng Y, Yu C R and You J C 2006 *J. At. Mol. Phys.* **23** 1111 (in Chinese)
[14] Held W D, Piper E, Ringer G and Toennies J P 1980 *Chem. Phys. Lett.* **75** 260
[15] Zhang Y and Shi H Y 2002 *J. Mol. Struct.* (theochem) **589** 89
[16] Murdachaew G, Szalewicz K, Jiang H and Bacic Z 2004 *J. Chem. Phys.* **121** 11839
[17] Yu C R, Huang S Z, Feng E Y, Wang R K, Cheng X L and Yang X D 2006 *Acta Phys. Sin.* **55** 2215 (in Chinese)
[18] Sun G H, Yang X D, Zhu J and Wang C X 2002 *Chin. Phys.* **11** 910
[19] Lotrich V F, Wormer P E S and Avoird A 2004 *J. Chem. Phys.* **120** 93
[20] Qiu M H, Ren Z F, Che L, Dai D X, Harich S A, Wang X Y and Yang X M 2006 *Chin. J. Chem. Phys.* **19** 93
[21] Yu C R 2006 *J. At. Mol. Phys.* **23** 310 (in Chinese)
[22] Yu C R, Feng E Y, Wang R K and Yang X D 2006 *Chin. Phys.* **15** 2571
[23] Yu C R, Wang R K, Cheng X L and Yang X D 2007 *Acta Phys. Sin.* **56** 2577 (in Chinese)
[24] Yu C R, Feng E Y, Cheng X L and Yang X D 2007 *Acta Phys. Sin.* **56** 4441 (in Chinese)
[25] Barton A E, Howlett D J B and Howard B J 1980 *Mol. Phys.* **41** 619
[26] Huston J M and Howard B J 1982 *Mol. Phys.* **45** 769
[27] Lovejoy C M and Nesbitt D J 1988 *Chem. Phys. Lett.* **147** 490
[28] Hutson J M 1989 *J. Chem. Phys.* **91** 4448
[29] Dudley T J, Pandey R R, Staffin P E, Hoffmann M R and Schatz G C 2001 *J. Chem. Phys.* **114** 6166
[30] Li J, Zhu H, Xie D Q and Yan G S 2003 *Chem. J. Chinese Universities* **24** 686
[31] Fajin J L, Cacheiro J L and Fernandez B 2004 *J. Chem. Phys.* **121** 4599
[32] Choi B H and Tang K T 1975 *J. Chem. Phys.* **63** 1775
[33] Huxley P, Knowels P B, Murrell J N and Watts J D 1984 *J. Chem. Soc. Faraday Trans.* II **80** 1349
[34] Bransden B H 1983 *Atomic Collision Theory* (Boston, MA: Benjamin Cummings) p12
[35] Yu C R, Huang S Z, Wang R K and Yang X D 2007 *Journal of University of Science and Technology of China* **37** 255 (in Chinese)
[36] Yu C R, Huang S Z, Shi S H, Cheng X L and Yang X D 2007 *Acta Phys. Sin.* **56** 5739 (in Chinese)
[37] Yu C R, Cheng X L and Yang X D 2007 *Chin. Phys. Lett.* **24** 1234